Monte Carlo Calculations for Alcohols and Their Mixtures with Alkanes. Transferable Potentials for Phase Equilibria. 5. United-Atom Description of Primary, Secondary, and Tertiary Alcohols

Bin Chen,[†] Jeffrey J. Potoff,[‡] and J. Ilja Siepmann*

Departments of Chemistry and Chemical Engineering and Materials Science, University of Minnesota, 207 Pleasant Street SE, Minneapolis, Minnesota 55455-0431

Received: October 20, 2000

The transferable potentials for phase equilibria-united atom (TraPPE-UA) force field for hydrocarbons is extended to primary, secondary, and tertiary alcohols by introducing the following (pseudo-)atoms: common hydroxyl O and H for all alcohols, α-CH_3, α-CH_2, α-CH, and α-C for methanol, primary, secondary, and tertiary alcohols, respectively. In the TraPPE-UA force field, the nonbonded interactions of these sites are governed by Lennard−Jones 12−6 potentials and Coulombic interactions of fixed partial charges. The values of these partial charges were borrowed from the optimized potentials for liquid simulations-united atom (OPLS−UA) force field [Jorgensen, W. L. *J. Phys. Chem.* **1986**, *90*, 1276]. The Lennard−Jones well depth and size parameters for the new interaction sites were determined by fitting to the single-component vapor−liquid-phase equilibria of a few selected model compounds. Although the well-depth parameters for the α-carbons could be taken directly from the TraPPE-UA parameters for the corresponding pseudoatoms in alkanes, the size parameters required small adjustments to reflect the differences in C−C and C−O bond lengths and the reduced electron density for α-carbons. Coupled−decoupled configurational-bias Monte Carlo simulations in the Gibbs and grand-canonical ensembles were carried out to calculate the one-component vapor−liquid coexistence curves for methanol, ethanol, propan-1-ol, propan-2-ol, butan-2-ol, 2-methylpropan-2-ol, pentan-1-ol, pentane-1,5-diol, and octan-1-ol, and to determine the binary phase diagrams for the mixtures of *n*-hexane/methanol and *n*-hexane/ethanol. It was found that the phase equilibria of the pure alcohols are accurately described by the TraPPE-UA force field, with mean unsigned deviations of about 1% from the experimental data for the normal boiling points and the saturated liquid densities. The azeotropic compositions for *n*-hexane/methanol and *n*-hexane/ethanol were predicted to be 0.340 at $T = 448.15$ K and 0.454 at 413.15 K and (in mole fraction of *n*-hexane), which are in good agreement with the experimental results of 0.288 and 0.440, respectively. Analysis of the structures of the *n*-hexane/methanol mixtures shows evidence for significant enhancements in the local mole fraction of alcohols in the vicinity of other alcohols. The magnitude of these local enhancements decreases with increasing alcohol concentration, but the change is gradual and no discontinuity was observed at the azeotropic composition.

1. Introduction

Alcohols are amphiphilic molecules composed of a flexible, nonpolar alkyl "tail" and a polar hydroxyl "head" that is capable of acting as hydrogen bond donor and acceptor. The formation of hydrogen-bonded clusters and networks leads to microheterogeneous liquid structures for the alcohols and deviations from ideal thermodynamic behavior (in particular, for mixtures with alkanes).[1,2] Alcohols are one of the most important classes of organic solvents because their amphiphilic nature leads to desirable solvent characteristics and because they are readily available. The thermodynamic properties of alcohols have been investigated in numerous experimental, computational, and theoretical studies (e.g., see refs 1−20). In addition, octan-1-ol/water partition coefficients are the main ingredient of quantitative structure−activity relationships[21,22] and are used to correlate or predict a plethora of other solute properties.[23]

Knowledge of the fluid phase diagrams and related thermophysical properties of the alcohols is essential in process design and optimization for practical applications. However, reliable experimental data are only available for relatively low molecular weight alcohols and only over a limited temperature range because of their thermal instability above 600 K. Molecular simulation is an alternative approach to investigate the microscopic structures and the thermophysical properties of the alcohols. In particular, because classical molecular mechanics type models are not subject to pyrolysis, simulations of these models can be used for prediction of the critical points and other coexistence properties of high-molecular-weight molecules.[24] However, the accuracy of the predictions obtained from simulations is limited by the quality of the molecular force field used to describe the model system. In a recent paper,[17] van Leeuwen reported on calculations of the vapor−liquid coexistence curves from methanol to hexanol obtained for the commonly used OPLS (optimized potential for liquid simulation) force field developed by Jorgensen[13] and for a force field that was derived

* To whom correspondence should be addressed. E-mail: siepmann@chem.umn.edu.

[†] Present address: Department of Chemistry, University of Pennsylvania, Philadelphia, PA 19104−6323.

[‡] Present address: Department of Chemical Engineering and Materials Science, Wayne State University, 5050 Anthony Wayne Drive, Detroit, MI 48202.

10.1021/jp003882x CCC: $20.00
Published on Web 03/24/2001

by van Leeuwen by combining the OPLS partial charges with Lennard−Jones (LJ) parameters from her own methanol force field[16] and the alkyl groups of the SKS force field.[24] It was found that the OPLS alcohol force field[13] is not transferable to the longer alcohols and to elevated temperatures. The force field proposed by van Leeuwen[17] performed much better but required fine-tuning of the methyl group parameters for each alcohol. Similarly, the exp-6 force field for methanol and ethanol recently discussed by Errington and Panagiotopoulos[19] makes use of different parameters for the hydroxyl O of these two alcohols.

A few years ago, this group started an effort to develop the transferable potentials for phase equilibria (TraPPE) force fields.[25−28] Saturated alkanes were the main focus in the first three papers in this series, and a computational efficient united-atom force field (TraPPE-UA) was developed for linear and branched alkanes.[25,26] In addition, united-atom parameters were determined for alkenes and alkylbenzenes.[28] The purpose of the TraPPE force fields is not only to be able to reproduce thermophysical properties over a wide range of physical conditions, but also to keep the models as transferable as possible by minimizing the number of different (pseudo-)atoms needed for any particular molecule and by using the same parameters for a given (pseudo-)atom in all types of molecules. In particular, for the united-atom version, this requires further explanation. Our philosophy in defining a given pseudo-atom is that it mimics the interactions of its core electrons plus a share of the valence electrons that make its bonds to the neighboring atoms. Actually, the contribution of the valence electrons far outweighs the contribution of the core electrons to the molecular polarizability.[29−31] For example, the pseudo-atom for a methyl group, that is connected to another carbon atom, accounts for the three C−H bonds and a share of one C−C bond (plus its core electrons). Thus, the same pseudo-atom is used for the methyl group in ethane, propane, or propene. However, the pseudo-atom for a methyl group connected by a single bond to an oxygen atom (say, in methanol) is different because it mimics the interactions of three C−H bonds and a share of one C−O bond. Clearly, differences in electronegativity between C and O atoms lead to intramolecular charge transfer and require the use of partial charges. However, because the polarizability of the valence electrons in the C−H bonds dominates the polarizability of the methyl pseudo-atom,[25−27,29−31] one might expect that to first order the polarizabilities (and the LJ well depths) of a methyl pseudo-atom in ethane and methanol are the same, whereas the sizes (LJ diameters) should differ because of the differences in C−C and C−O bond lengths[26] and the electron withdrawing effect of the hydroxyl oxygen.[32]

To model methanol, primary, secondary, and tertiary alcohols, we need to introduce the following (pseudo-)atoms: common hydroxyl O and H for all alcohols, α-CH_3, α-CH_2, α-CH, and α-C for the different α-carbon groups. The remainder of this article is arranged as follows. Sections 2 and 3 give descriptions of the TraPPE-UA alcohol force field and the simulation details, respectively. In the first part of section 4, the performance of the new model for single-component vapor−liquid coexistence curves is discussed. Thereafter, we present simulation results for the mixtures of *n*-hexane/methanol and *n*-hexane/ethanol. Finally, conclusions are made in section 5.

2. Force Field Development

In the TraPPE-UA force field, CH_x groups (e.g., methyl, methylene, or aromatic CH) are treated as pseudoatoms located at the sites of the carbon atoms, whereas all other atoms (e.g., hydroxyl O and H) are modeled explicitly. The nonbonded interactions are described by pairwise-additive LJ 12−6 potentials and Coulombic interactions of partial charges

$$u(r_{ij}) = 4\epsilon_{ij}\left[\left(\frac{\sigma_{ij}}{r_{ij}}\right)^{12} - \left(\frac{\sigma_{ij}}{r_{ij}}\right)^{6}\right] + \left\{\frac{q_i q_j}{4\pi\epsilon_0 r_{ij}}\right\} \qquad (1)$$

where r_{ij}, ϵ_{ij}, σ_{ij}, q_i, and q_j are the separation, LJ well depth, LJ size, and partial charges, respectively, for the pair of atoms *i* and *j*. Lorentz−Berthelot combining rules[33,34] are used to determine the parameters for unlike LJ interactions. As is customary, the nonbonded potentials of eq 1 are used only for the interactions of pseudo-atoms belonging to different molecules or belonging to the same molecule but whose interactions are not accounted for by any of the intramolecular, bonded potentials: fixed bond lengths for neighboring pseudo-atoms, harmonic bond bending potentials for pseudo-atoms separated by two bonds, and dihedral potentials for pseudo-atoms separated by three bonds. It must be emphasized here that this simple division between nonbonded and bonded interactions requires caution for multifunctional, polar molecules. For example, in propane-1,3-diol the proximity of the two polar groups leads to problems. If one excludes the usual 1−3 and 1−4 nonbonded intramolecular interactions, then only the Coulombic interactions of two O−H groups with negative net charge remain. This would disfavor intramolecular hydrogen bonding. Nevertheless, if one uses the full set of Coulombic interactions including 1−3 and 1−4 interactions, then the close proximity of the positively charged α-carbons leads to an unphysical widening of the C−C−C bond angle. Thus, different interaction parameters (both bonded and nonbonded) would be required to model bifunctional alcohols where the hydroxyl groups are either connected to the same α-carbon or separated by less than 5 carbon atoms. However, these bifunctional alcohols are not considered here and the TraPPE-UA force field should not be used for them (without modifications).

In the TraPPE-UA force field, all bond lengths are fixed. The bond lengths for the O−H, CH_x-O, and CH_x-CH_y single bonds are listed in Table 1. A harmonic potential is used to control bond angle bending

$$u_{\text{bend}} = \frac{k_\theta}{2}(\theta - \theta_0)^2 \qquad (2)$$

where θ, θ_0, and k_θ are the measured bending angle, the equilibrium bending angle, and the force constant, respectively. Table 1 contains a list of the θ_0 and k_θ parameters used here, where the k_θ value for the C−C−C bending angles were taken from the work of van der Ploeg and Berendsen,[35] and the values for the C−C−O and C−O−H bending angles were taken from the AMBER94 force field.[36]

The torsional potentials used to restrict the dihedral rotations around bonds connecting two methylene pseudo-atoms and around bonds connecting a methylene pseudo-atom with a CH-(sp^2) were taken from the OPLS−UA force field[13,37]

$$u_{\text{tors}} = c_0 + c_1[1 + \cos(\phi)] + c_2[1 - \cos(2\phi)] + c_3[1 + \cos(3\phi)] \qquad (3)$$

with the Fourier coefficients listed in Table 1.

Following the TraPPE philosophy described above, the nonbonded interaction parameters for the six new pseudoatoms (hydroxyl O and H, α-CH_3, α-CH_2, α-CH, and α-C) were determined as follows. Because the hydroxyl H is always bonded to the hydroxyl O and the hydroxyl O is always bonded to a

TABLE 1: Bonded and Nonbonded Parameters for the TraPPE-UA Alcohol Force Field

stretch	r_0 [Å]		
CH_x-CH_y	1.54		
CH_x-OH	1.43		
O−H	0.945		
bend (eq 2)	**θ_0 [deg]**	**k_θ/k_B [K]**	
$CH_x-(CH_2)-CH_y$	114	62 500	
$CH_x-(CH)-CH_y$	112	62 500	
$CH_x-(C)-CH_y$	109.47	62 500	
$CH_x-(CH_y)-O$	109.47	50 400	
$CH_x-(O)-H$	108.5	55 400	
torsion (eq 3)	**c_0/k_B [K]**	**c_1/k_B [K]**	**c_2/k_B [K]**	**c_3/k_B [K]**
$CH_x-(CH_2)-(CH_2)-CH_y$	0	335.03	−68.19	791.32
$CH_x-(CH_2)-(CH_2)-OH$	0	176.62	−53.34	769.93
$CH_x-(CH_2)-(O)-H$	0	209.82	−29.17	187.93
$CH_x-(CH)-(O)-H$	215.96	197.33	31.46	−173.92
$CH_x-(C)-(O)-H$	0	0	0	163.56
nonbonded (eq 1)	**ϵ/k_B [K]**	**σ [Å]**	**q**	
$CH_x-(O)-H$	93	3.02	−0.700	
O−(H)			+0.435	
$(CH_3)-OH$	98	3.75	+0.265	
$(CH_3)-CH_x$	98	3.75		
$CH_x-(CH_2)-OH$	46	3.95	+0.265	
$(CH_x)_2-(CH_2)$	46	3.95		
$(CH_x)_2-(CH)-OH$	10	4.33	+0.265	
$(CH_x)_3-(CH)$	10	4.68		
$(CH_x)_3-(C)-OH$	0.5	5.80	+0.265	
$(CH_x)_4-(C)$	0.5	6.40		

carbon atom, there should only be one common set of parameters for the hydroxyl O and H atoms for all alcohols. The partial charges for these two atoms (and the compensating charge for the α-carbon to maintain molecular neutrality) were borrowed directly from the OPLS−UA force field.[13] Using a common set of partial charges for all alcohols is clearly an oversimplification because it ignores the influence of the alkyl tail on the electronic structure of the hydroxyl group. It is well-known that gas-phase dipole moments differ among the alcohols (e.g., decrease with increasing chain length for the primary alcohols).[38] Furthermore, using fixed charges ignores many-body polarization effects.[31,39] A polarizable model, such as those for water,[40] would be required to account for different environments, such as those encountered in the vapor phase versus the liquid phase or in dilute versus concentrated solutions of alcohols in alkanes.

Given the set of fixed charges for the hydroxyl O and H and the α-carbons, we can now shift our attention to the determination of the LJ parameters. The new LJ parameters for the hydroxyl O (see Table 1) were obtained from calculations of the vapor−liquid equilibria for methanol and ethanol using the LJ parameters of the alkane methyl and methylene groups for the α-carbons without modification. In principle, these α-CH_3 and α-CH_2 parameters might differ slightly from the corresponding alkane parameters because of the difference of the C−O and C−C bond lengths and bond polarizabilities. However, fitting the LJ parameters for multiple pseudoatoms in the same molecule is an arduous task. Thus, we decided to focus on the hydroxyl O (the effective parameter of which can also be viewed as accounting for the small changes in the α-CH_3 and α-CH_2 pseudoatoms). The transferability of the α-CH_2 parameters was then tested by carrying simulations for some longer primary alcohols and for pentane-1,5-diol.

Finally, using the LJ parameters for the hydroxyl O obtained from simulations for methanol and ethanol, the LJ parameters for the α-CH and α-C pseudoatoms in secondary and tertiary alcohols were determined from simulations for propan-2-ol and 2-methylpropan-2-ol, respectively. Short test simulations showed that use of the corresponding alkane LJ parameters without modifications would lead to significantly too low saturated liquid densities. This does not come as a surprise because the diameters of the alkane CH and C pseudoatoms are relatively large which severely impacts on the ability of these alcohols to form hydrogen bonds. (In addition, the set of LJ parameters for the methine and quaternary carbon, that were fitted for neopentane and isobutane, were found to work less satisfactorily for 2,3-dimethylbutane and 2,2-dimethylhexane.[26]) As discussed in the Introduction, it is expected that the replacement of a C−C bond with a shorter C−O bond and the electron withdrawing effect of the hydroxyl oxygen should mainly affect the diameters of the α-CH and α-C pseudoatoms, whereas the changes for the well depths should be smaller. Thus, only the σ parameters for these groups were adjusted to fit the phase diagrams of propan-2-ol and 2-methylpropan-2-ol. The parameters for all α-carbon pseudoatoms and the corresponding alkane pseudoatoms are listed in Table 1.

3. Simulation Details

A. Single-Component Vapor−Liquid Coexistence Curves. A combination of the Gibbs ensemble Monte Carlo method (GEMC)[41−43] and the coupled−decoupled configurational-bias Monte Carlo (CBMC) algorithm[26,44−48] was employed to calculate the vapor−liquid coexistence curves (VLCCs) for the following alcohols (system sizes in brackets): methanol (500 molecules), ethanol (300), propan-1-ol (200), propan-2-ol (200), butan-2-ol (240), 2-methylpropan-2-ol (200), pentan-1-ol (150), pentane-1,5-diol (150), and octan-1-ol (120). The combined volume of the two simulation boxes was adjusted to yield liquid-phase simulation boxes with linear dimension of about 30 Å and larger vapor phases containing at least 10 molecules. For the LJ part of the potential, a spherical potential truncation for pairs of pseudo-atoms separated by more than 14 Å was enforced, and analytic tail corrections (for energies, pressures, and chemical potentials) were employed.[49,50] However, an Ewald sum with tin-foil boundary conditions ($\kappa \times L = 5$ and $K_{max} = 5$) was used for the long-range electrostatic part of the potential.[50]

For a given alkanol, the initial configuration was constructed as a layered crystal structure.[51] Several thousand Monte Carlo cycles (N moves) at elevated temperature were used to "melt" the crystal structure, and the system was then "cooled" to the desired temperature. Only translational, rotational, and conformational moves were employed during the melting and cooling periods. Thereafter, the system was allowed to equilibrate for at least 10 000 Monte Carlo cycles followed by a production run of 50 000 Monte Carlo cycles. Five different Monte Carlo moves were used to sample phase space in the Gibbs ensemble simulations. In addition to the translational, rotational, and conformational moves, volume exchanges and particle swaps between the two boxes were carried out to allow the two-phase system to equilibrate the pressure (mechanical equilibrium) and the chemical potential (phase equilibrium). Moves were selected randomly with fixed probabilities that were adjusted to yield about one accepted particle swap or volume exchange per 10 Monte Carlo cycles, and the remainder of the moves were equally divided among the translational, rotational, and conformational moves. Standard deviations of the ensemble averages were computed by breaking the production runs into five blocks.

The coupled−decoupled CBMC algorithm[26] was used for conformational and particle-swap moves. Computational efficiency was improved by utilizing a biased insertion with 10 trial sites for the first interaction site in a CBMC particle swap,[52,53] an additional center-of-mass based cutoff which avoids computing unnecessary distances,[25] and a shorter potential truncation ($r_{CBMC} = 5$ Å) for use during split-energy CBMC moves[48] which is then corrected to the full potential ($r_{cut} = 14$ Å) with tail corrections in the acceptance rule. A coupled−decoupled CBMC particle swap of the alcohols proceeds as follows: First, the hydroxyl O is inserted (using multiple insertions). Second, the hydroxyl H and α-carbons are added concomitantly. Thereafter, the remainder of the alkyl tail is grown.

B. Vapor−Liquid Coexistence Curves for Binary Mixtures. Coupled-decoupled CBMC simulations in the grand canonical ensemble were used to determine the pressure-composition diagrams for *n*-hexane/methanol and *n*-hexane/ethanol mixtures. Histogram reweighting techniques were used to construct the phase diagrams from probability distributions extracted from the simulations.[54−59] The implementation of this methodology for binary mixtures has been described in detail[58,59] and is not repeated here. A box length of $L = 22$ Å was used for all simulations. The LJ interactions were truncated at a distance of $L/2$ and analytical tail corrections were used. In addition, an Ewald sum with the same parameters as in the GEMC simulations was used. Equilibration periods consisted of more than 1 million Monte Carlo steps (MCS). Vapor-phase simulations were run for 5 million MCS, whereas simulations in the liquid phase extended over 10−20 million MCS. Simulation data were stored in the form of lists containing the number of molecules of each species and the energy of the system. Samples were written to these lists every 500 MCS.

C. Structural Properties for Binary Mixtures. Simulations in the isothermal−isobaric (*NpT*) ensemble were used to investigate the structural properties of the liquid phase of the mutually saturated *n*-hexane/methanol mixtures. 200 Molecules were used for each simulation. Simulations were equilibrated for 50 000 MC cycles, and the production periods covered an additional 50 000 MC cycles. The type of move was selected at random and the probabilities of the different moves were set to 0.01 for volume changes and 0.33 for translational, rotational, or conformational moves. The LJ interactions were truncated at 11 Å and analytical tail corrections were applied. An Ewald sum with the same parameters as used in the GEMC simulations was used to estimate the long-range electrostatic interactions.

4. Results and Discussion

A. Single-Component Vapor−Liquid Coexistence Curves. The VLCCs for five primary alcohols (methanol, ethanol, propan-1-ol, pentan-1-ol, and octan-1-ol), two secondary alcohols (propan-2-ol and butan-2-ol), one tertiary alcohol (2-methylpropan-2-ol), and one bifunctional alcoholol (pentane-1,5-diol) were calculated using the TraPPE-UA force field. The results for the saturated vapor pressures, vapor and liquid densities, and the heats of vaporization are listed in Table 2 and compared to the available experimental data[60,61] in Figures 1 to 3. The experimental saturated liquid densities are very well reproduced with average deviations of about 1%. However, larger deviations were observed for the saturated vapor densities and pressures. As can be seen from the Clausius−Clapeyron plots (see Figure 2), the vapor pressures are overestimated at higher reduced temperatures but underestimated at lower reduced temperatures. This behavior is more pronounced for the low-molecular-weight alcohols. Here, it should be recalled that the TraPPE-UA force field yields saturated vapor pressures for unsaturated alkanes that are too high over the entire coexistence range.[25,26] Significant deviations are also found for the heats of vaporization (see Figure 3). For example, the heats of vaporization for ethanol are slightly too low below the boiling point but too high above it. The calculated heats of vaporization for octan-1-ol deviate significantly from their experimental counterparts. However, the rather linear shape of the experimental heat of vaporization curve allows for some doubts on its validity.

The normal boiling points and critical constants estimated using the TraPPE-UA force field and their experimental counterparts are listed in Table 3 and scatter plots for the boiling and critical temperatures are shown in Figure 4. The normal boiling points can be directly obtained from interpolation of the data in the Clausius−Clapeyron plots. In contrast, the estimation of the critical constants is less direct. These properties were obtained from least-squares fits of the saturated vapor and liquid densities to the scaling law and the law of rectilinear diameters.[62,63] However, although this procedure works rather well for rare gases[62] and alkanes,[25,26] the range of applicability of the scaling law is more limited for polar molecules, such as the alcohols or water, as can be inferred from the different shapes of the coexistence curves.[64] Thus, we estimated effective scaling exponents, β^*, from least-squares fits (constrained to reproduce the experimental critical temperatures and densities) of the experimental data at the same temperatures as used in the GEMC simulations. The β^* show very little variation among the alcohols (see Table 3), but are significantly smaller than the universal Ising value of 0.325. We feel that the use of this ad hoc procedure is justified given the approximate nature of nonpolarizable united-atom force fields. More precise estimates of the critical properties can be achieved by using the grand-canonical ensemble simulations combined with histogram-reweighting and a mixed-field scaling analysis.[58,65] Although this procedure is straightforward for a given system size, estimation of the infinite-size limit of the critical constants becomes an arduous task because it requires simulations over a wide range of system sizes.

The experimental normal boiling points are well reproduced with a mean unsigned deviation of less than 1% (see Figure 4). Agreement for the critical constants is satisfactory: the critical temperatures of most alcohols are slightly underestimated with an average deviation of about 1.5%, whereas the critical densities are overestimated on average by about 3%. The latter disagreement originates from two separates causes. First, because the law of rectilinear diameters has a negative slope, an underestimation of the critical temperatures results in an overestimation of the critical densities. Second, whereas the saturated liquid densities are reproduced well, the vapor densities at elevated temperatures are too high, which results in a shift of the mean saturated densities to higher values. Nevertheless, the overall accuracy of the predictions for vapor−liquid-phase equilibria calculated with the TraPPE-UA force field is very encouraging and a substantial improvement over other general purpose molecular mechanics force fields.[17] It is striking that good results can be obtained for the VLCC of methanol and ethanol given the fact that the LJ parameters for the methyl and methylene pseudoatoms were taken directly from the alkane force field and that a common set of partial charges was used. The TraPPE-UA force field reproduces also the relatively small differences between propan-1-ol (a primary alcohol), propan-2-ol (a secondary alcohol), and 2-methylpropan-2-ol (a ternary alcohol).

TABLE 2: Numerical Results of the Gibbs-Ensemble Simulations for Pure Alcohols Using the TraPPE-UA Force Field[a]

T	P	ρ_{vap}	ρ_{liq}	H_{vap}	P	ρ_{vap}	ρ_{liq}	H_{vap}
		methanol				ethanol		
275	0.0038_2	$0.000\,054_3$	0.807_2	41.0_2	0.0014_2	$0.000\,029_3$	0.804_2	44.7_2
300	0.017_1	$0.000\,23_1$	0.782_1	39.5_2	0.0081_5	$0.000\,15_1$	0.782_1	43.3_1
325	0.052_2	$0.000\,65_3$	0.753_2	37.5_2	0.030_3	$0.000\,52_5$	0.756_2	41.5_2
375	0.354_7	0.0042_2	0.692_7	32.8_4	0.234_{10}	0.0040_3	0.705_3	36.3_2
425	1.57_5	0.021_1	0.628_3	25.2_7	1.11_5	0.018_1	0.635_3	29.4_6
475	4.96_4	0.110_5	0.518_8	12.7_5	3.2_2	0.054_5	0.524_4	21.2_6
		propan-1-ol				pentan-1-ol		
300	0.0045_2	$0.000\,11_1$	0.792_1	47.6_1	$0.000\,46_4$	$0.000\,016_1$	0.807_2	55.7_1
350	0.043_1	$0.000\,92_6$	0.744_2	43.4_2	0.0103_4	$0.000\,32_1$	0.769_2	51.4_2
400	0.374_{15}	0.0077_6	0.702_2	36.9_2	0.091_4	0.0025_1	0.723_2	45.2_2
450	1.21_3	0.025_2	0.628_4	29.5_4	0.407_{25}	0.0104_6	0.660_4	38.1_2
500	3.39_{15}	0.086_9	0.512_7	16.23_6	1.24_3	0.032_1	0.590_3	29.4_3
515	3.85_{19}	0.094_8	0.376_4	13_2				
550					2.94_{14}	0.094_{10}	0.495_{11}	19.1_5
565					3.52_{10}	0.120_8	0.439_{16}	15.0_4
		octan-1-ol				propan-2-ol		
300	$0.000\,018_2$	$0.000\,000\,81_3$	0.824_2	69.2_1	0.0040_5	$0.000\,14_1$	0.779_2	45.6_1
350	0.0008_1	$0.000\,034_6$	0.789_2	64.2_2	0.098_9	0.0022_2	0.732_3	40.2_4
400	0.012_1	$0.000\,50_6$	0.743_2	56.7_2	0.52_4	0.012_1	0.661_4	31.8_9
450	0.083_3	0.0030_2	0.698_2	50.1_2	1.77_6	0.039_3	0.566_5	24.1_2
490					3.7_5	0.102_{12}	0.388_{20}	12.1_7
500	0.31_1	0.0107_3	0.640_2	41.5_3				
550	0.81_4	0.029_2	0.572_3	32.7_5				
600	1.64_7	0.063_3	0.469_6	23.1_3				
		butan-2-ol				2-methylpropan-2-ol		
300	0.0034_1	$0.000\,101_3$	0.794_2	49.2_2	0.0063_3	$0.000\,19_1$	0.779_1	44.7_1
350	0.043_2	0.0011_1	0.751_2	44.9_2	0.113_8	0.0030_2	0.723_2	38.3_2
400	0.32_2	0.0083_5	0.693_3	37.0_3	0.661_{23}	0.017_1	0.660_3	30.2_4
450	1.11_5	0.026_1	0.609_4	28.1_4	1.72_{15}	0.052_7	0.557_{10}	21.2_4
480					3.7_2	0.156_3	0.156_3	11.0_6
500	3.2_1	0.100_7	0.483_8	16.0_5				
		pentane-1,5-diol						
500	0.077_5	0.0020_1	0.823_3	61.2_6				
550	0.32_2	0.0078_5	0.771_2	53.4_4				
600	0.90_2	0.022_1	0.705_2	44.8_2				
650	2.1_1	0.061_6	0.621_5	33.3_7				

[a] Temperatures, saturated vapor pressures, orthobaric densities, and heats of vaporization are given in units of K, MPa, g/mL, and kJ/mol, respectively. The subscripts give the statistical accuracies of the last decimal(s).

Finally, the large differences between pentan-1-ol and pentane-1,5-diol are also accurately reproduced.

B. Microscopic Structures of the Pure Liquid Phases. It is well-known[1,2] that the amphiphilic character of the alcohols leads to a unique microheterogeneous environment in the liquid phases, characterized by the formation of locally oriented, polar regions consisting of hydrogen-bonded clusters of the hydroxyl headgroups which are embedded in isotropic, nonpolar regions consisting of the alkyl tails. Both an increase of the chain length (say, for the primary alcohols) or an enhancement of the bulkiness of the alkyl group (such as for primary, secondary, and tertiary alcohol isomers) raise the stress on the hydrogen-bonded network. As is evident from Figure 5, dramatic changes are evident in the calculated cluster-size distributions for propan-1-ol, propan-2-ol, 2-methylpropan-2-ol, and octan-1-ol. (The cluster size was determined using a cutoff distance of 3.5 Å for oxygen−oxygen separations.) For propan-1-ol and propan-2-ol, we found broad and nearly uniform cluster-size distributions. For the 2-methylpropan-2-ol phase, in contrast, about 40% of the molecules belong to clusters with an aggregation number of 4 and relatively few clusters with aggregation numbers higher than 20 were found. The cluster-size distribution for the liquid octan-1-ol phase, is broad but with a noticeable peak for aggregation numbers between 4 and 10. It should be noted here, that the statistical noise in the cluster-size distributions is significant, because changes in aggregation numbers are mainly sampled via the (few) particle swap moves, whereas translational and rotational moves are less efficient in moving a molecule from one cluster to another.

Regardless of the differences in the cluster-size distributions, it was found that the overwhelming majority of hydroxyl groups participates in the formation of two hydrogen bonds for all nine alcohols studied here. The average numbers of hydrogen bonds per hydroxyl group (again calculated using a cutoff of 3.5 Å for the oxygen−oxygen separation, see also discussion below) are 2.07 (methanol), 2.03 (ethanol), 2.01 (propan-1-ol), 2.00 (propan-2-ol), 1.90 (2-methylpropan-2-ol), 2.06 (pentan-1-ol), and 2.07 (octan-1-ol). These values agree well with the experimental reports of coordination numbers of two for liquid methanol, ethanol,[3−5] propan-1-ol,[6] and 2-methylpropan-2-ol.[7] Nevertheless, whereas the number of hydrogen bonds per hydroxyl group does not change significantly with chain length or bulkiness of the alkyl group, the potential energy distributions for the headgroup interactions (calculated for pairs of neutral headgroups consisting of the hydroxyl O and H and the α-carbon) show more substantial differences (see Figure 6). The bimodal character of the bonding energy distributions clearly reflects a microscopic structure that is dominated by the formation of hydrogen-bonded clusters. Although the energetics of the hydrogen-bonded network are rather similar for propan-1-ol, octan-1-ol and propan-2-ol, there is a shift in the peak position of about 3 kJ/mol to less favorable energies for 2-methylpropan-2-ol. This shift in the hydrogen-bond energy distribution is mainly responsible for the loss in cohesive energy

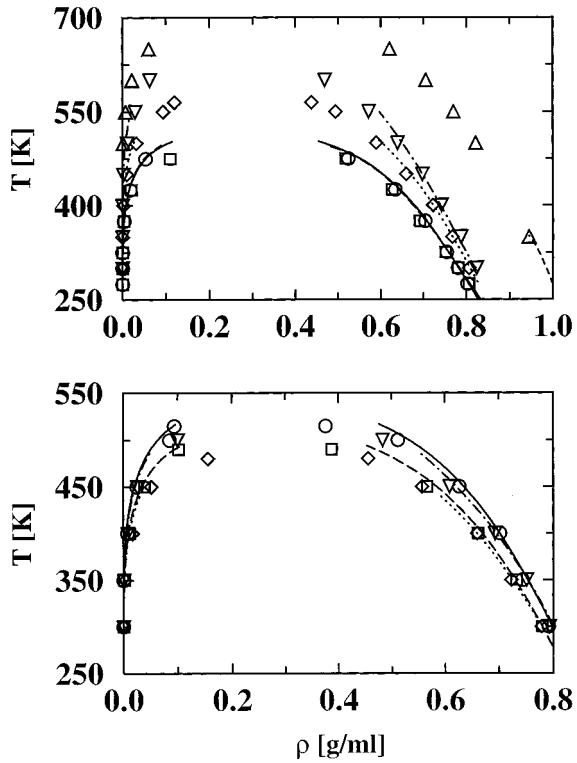

Figure 1. Vapor−liquid coexistence curves. Experimental data[60] and simulation results are shown as lines and symbols, respectively. Top: methanol (dashed lines and squares), ethanol (solid lines and circles), pentan-1-ol (dotted lines and diamonds), octan-1-ol (dash−dotted lines and triangles down), and pentan-1,5-diol (dashed lines and triangles up). Bottom: propan-1-ol (solid lines and circles), propan-2-ol (dashed lines and squares), butan-2-ol (dash−dotted lines and triangles down), and 2-methylpropan-2-ol (dotted lines and diamonds).

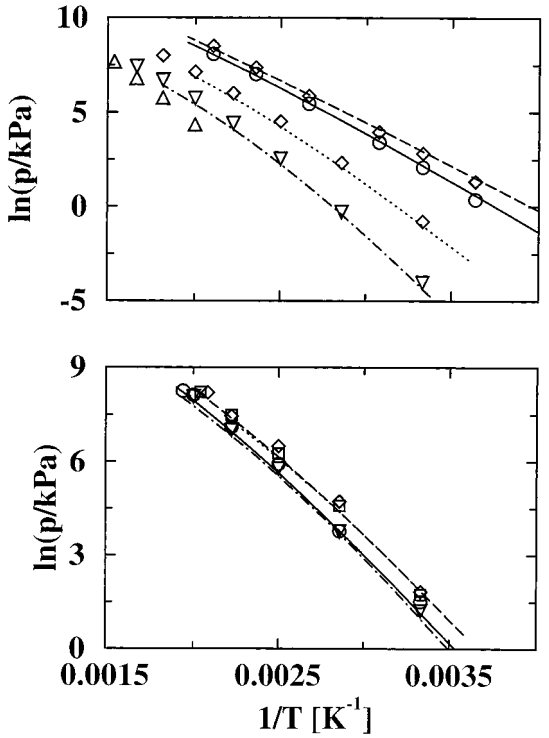

Figure 2. Clausius−Clapeyron plots of the saturated vapor pressure against the inverse temperature. Linestyles (for experimental data) and symbols (for simulation results) as in Figure 1.

observed for tertiary alcohols that leads to a lowering of their boiling points compared to primary and secondary alcohols of

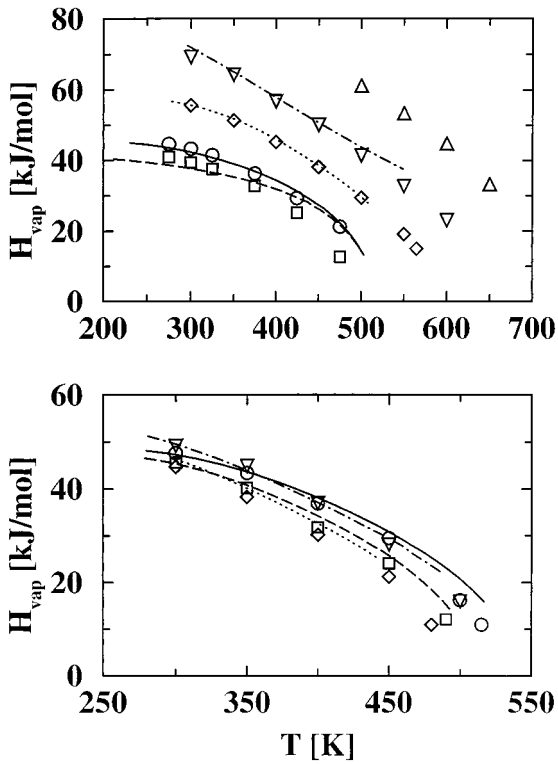

Figure 3. Heats of vaporization versus temperature. Linestyles (for experimental data) and symbols (for simulation results) as in Figure 1.

TABLE 3: Comparison of the Estimated normal Boiling Points (in K), Critical Temperatures (in K), and Critical Densities (in g/mL)[a]

		T_b	β^*	T_c	ρ_c
methanol	TraPPE-UA	340_1	0.28	502_2	0.285_4
	exp	338		513	0.272
ethanol	TraPPE-UA	353_1	0.28	514_2	0.281_3
	exp	351		514	0.276
propan-1-ol	TraPPE-UA	368_2	0.29	538_2	0.290_4
	exp	370		537	0.275
pentan-1-ol	TraPPE-UA	406_2	0.29	579_3	0.279_3
	exp	411		588	0.270
octan-1-ol	TraPPE-UA	460_3	0.29	629_2	0.270_2
	exp	468		652	0.266
propan-2-ol	TraPPE-UA	354_3	0.29	502_2	0.281_4
	exp	355		508	0.273
butan-2-ol	TraPPE-UA	370_3	0.29	524_2	0.287_4
	exp	373		536	0.276
2-methylpropan-2-ol	TraPPE-UA	354_4	0.29	504_3	0.283_5
	exp	355		506	0.270
pentane-1,5-diol	TraPPE-UA	508_2	0.29	710_3	0.311_4
	exp	512			

[a] β^* is the effective scaling exponent (see text). The subscripts give the statistical accuracies of the last decimal. The experimental data are taken from ref 60.

the same molecular weight. Furthermore, the low-energy side of the main peak (pair energies between −10 to −5 kJ/mol) arises from configurations of neighboring molecules that do not show a hydrogen bond but have a favorable orientation of the dipole vectors.

The strain on the formation of hydrogen bonds caused by the bulkiness of the *tert*-butyl tail group is also evident in the angular distribution of hydrogen-bonded pairs. Table 4 shows a comparison of the average numbers of hydrogen-bonded pairs in methanol and in 2-methylpropan-2-ol that were found within a certain oxygen−oxygen separation range and within a certain range for the angle, ϕ, formed by the oxygen−hydrogen bond

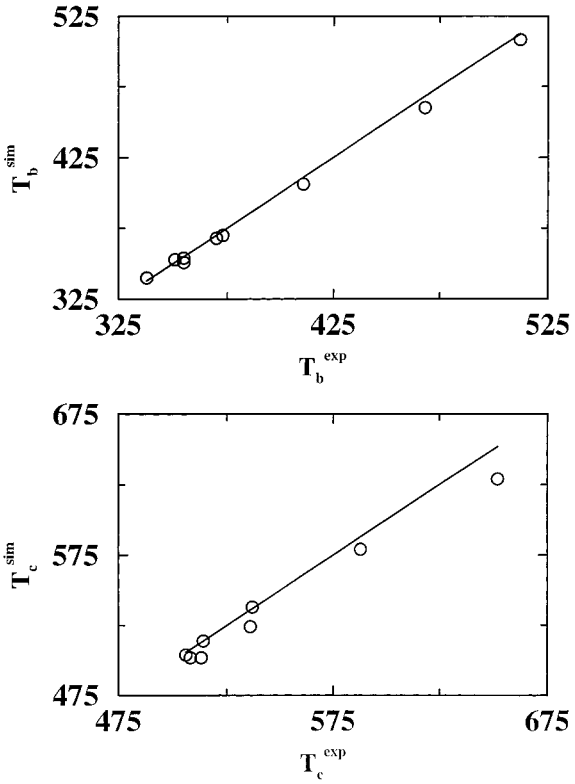

Figure 4. Correlation plot of the estimated simulation results versus the experimental data for the normal boiling point (top) and the critical temperature (bottom).

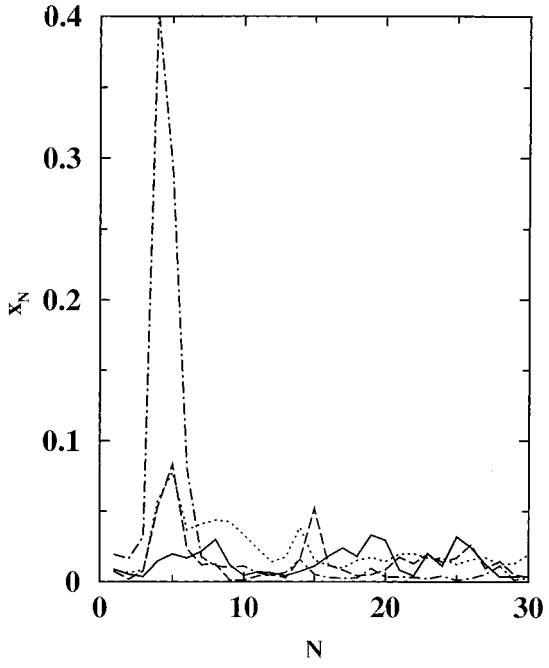

Figure 5. Fraction of molecules which belong to a cluster of a given aggregation number calculated for the saturated liquid phases at $T =$ 300 K. The distributions for propan-1-ol, propan-2-ol, 2-methylpropan-2-ol, and octan-1-ol are represented by the solid, dashed, dashed−dotted, and dotted lines.

vector of the hydrogen donor and the oxygen−(fictitious) lone pair vector of the acceptor. Only 30% of the hydrogen-bonded pairs in 2-methylpropan-2-ol possess close to optimal hydrogen-bond geometries (that satisfy $2.6 < r_{OO} \leq 3.0$ and $\cos \phi < -0.8$), whereas nearly 50% of the hydrogen-bonded pairs in methanol satisfy the criteria above. It is sometimes argued that

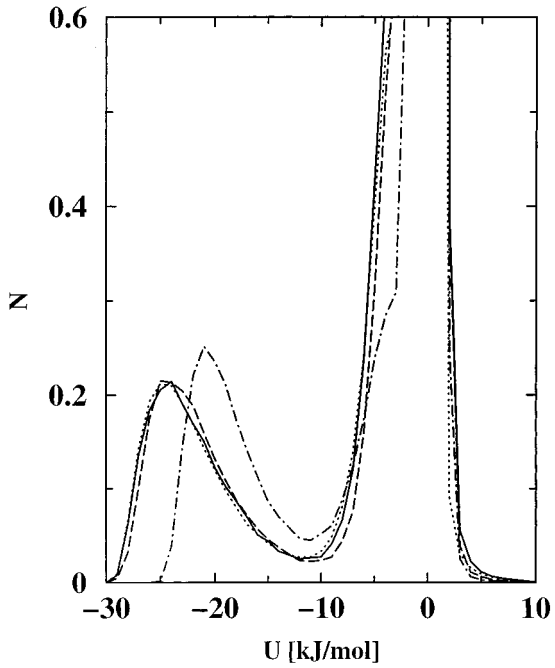

Figure 6. Potential energy distributions for headgroup−headgroup interactions calculated for the saturated liquid phases at $T =$ 300 K. Linestyles as in Figure 5.

a combined distance/angular cutoff should be used to determine the formation of a hydrogen bond, but for the simple force field used here any criterion will always remain ambiguous. In light of the experimental results[3−7] that assigned a coordination number of two to liquid methanol, ethanol, propan-1-ol and 2-methylpropan-2-ol, we decided to use a "loose" distance-based criterion throughout this work.

The oxygen−oxygen (OO), α-methylene−α-methylene (αα), and methyl−methyl (ee) radial distribution functions (RDFs) and corresponding number intergrals (NIs) for ethanol, pentan-1-ol, and octan-1-ol are plotted in Figures 7 and 8, respectively. Most noticeable are the large enhancements of the heights of the first peaks for the OO and αα RDFs from ethanol to octan-1-ol, whereas the peak positions remain at 2.7 and 4.5 Å, respectively. These results agree well with the X-ray diffraction experiments[3−7,9,11] and earlier simulation data for the OPLS alcohol force field.[13] The enhancements of the peak heights are mainly caused by the dilution of the average number densities for the headgroups by the nonpolar alkyl tails with increasing chain length. As is shown in Figure 8, the OO NIs for the three alcohols are very similar out to pair separations of about 4.5 Å, which encompasses the full first shell and part of the second shell of the hydrogen-bonded network. For pentan-1-ol and octan-1-ol, the OO NIs remain close even beyond the second shell (about 5.5 Å). This should not come as a surprise because the probabilities to observe clusters with fewer than five molecules are very small for all primary alcohols. The relative enhancements in the αα RDFs are significant but smaller than for the OO RDFs. As can be seen from the αα NIs, the steric hindrance of the alkyl tails leads to differences between the alcohols already for the numbers of nearest neighbor contacts.

The ee RDFs for pentan-1-ol and octan-1-ol do not show any special features and are in good agreement with those for the corresponding alkanes. Thus, the packing of the methyl end segments of these relatively long alcohols is not disturbed by the hydrogen-bonded network of the headgroups. In contrast, the first peak of the ee RDF for ethanol shows a visible shoulder that is not present in ethane. As should be expected for very

TABLE 4: Average Numbers (multiplied by 1000) of Hydrogen-Bonded Pairs in Pure Methanol and Pure 2-methyl-propan-2-ol Sorted by Oxygen−Oxygen Separation and Hydrogen Bond Angle[a]

	2.5;2.6	2.6;2.7	2.7;2.8	2.8;2.9	2.9;3.0	3.0;3.1	3.1;3.2	3.2;3.3	3.3;3.4	3.4;3.5	sum
						methanol					
−1.0;−0.8	126	299	324	233	132	71	43	29	21	22	1301
−0.8;−0.6	61	136	149	106	58	33	19	14	13	13	603
−0.6;−0.4	9	22	27	20	13	9	8	6	8	9	131
−0.4;−0.2	0	1	1	2	1	2	2	3	4	5	22
−0.2;0.0	0	0	0	0	0	0	1	3	2	4	11
sum	197	459	503	361	205	115	73	55	48	52	2068
						2-methylpropan-2-ol					
−1.0;−0.8	27	108	167	173	124	80	50	33	18	15	796
−0.8;−0.6	33	106	163	138	91	54	29	19	12	8	653
−0.6;−0.4	18	61	86	70	45	29	11	8	5	6	340
−0.4;−0.2	2	7	10	11	9	5	5	5	5	8	68
−0.2;0.0	0	1	2	3	2	4	5	5	7	9	39
sum	81	284	429	395	270	172	101	71	47	47	1896

[a] Where 2.5;2.6 stands for $2.5 < r_{OO} \leq 2.6$ and where −1.0; −0.8 stands for $-1.0 < \cos\phi \leq -0.8$ (r_{OO} and ϕ are the oxygen−oxygen separation and hydrogen bond angle, respectively).

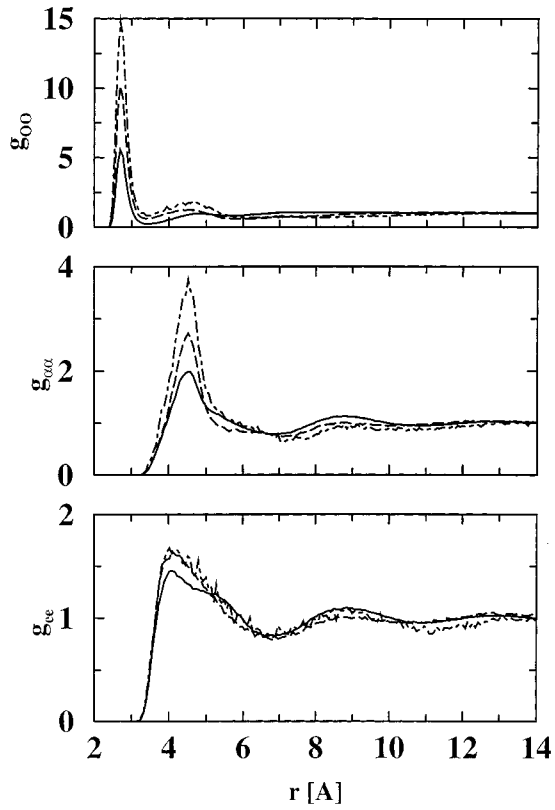

Figure 7. Oxygen−oxygen (top), α-methylene−α-methylene (middle), and methyl−methyl (bottom) radial distribution functions calculated for the saturated liquid phases of ethanol (solid lines), pentan-1-ol (dashed lines), and octan-1-ol (dashed−dotted lines) at $T = 300$ K using the TraPPE-UA alcohol force field.

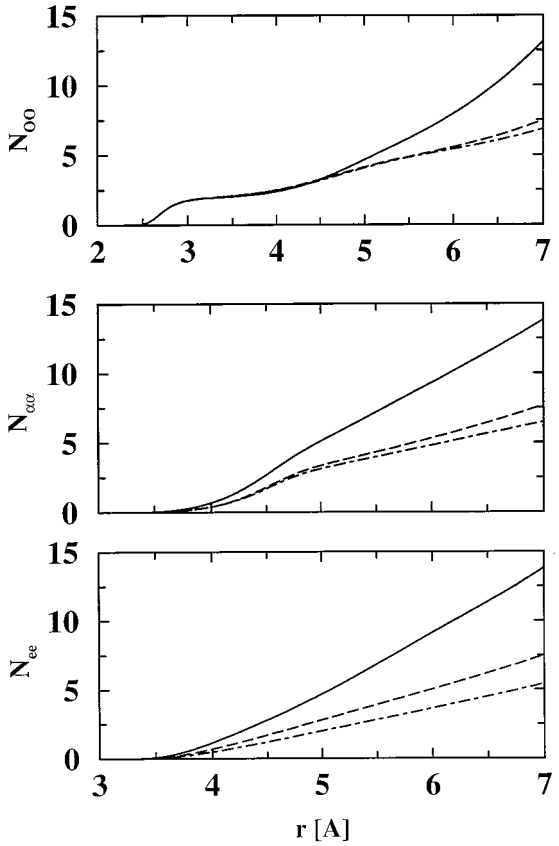

Figure 8. Number integrals for the radial distributions functions shown in Figure 7.

short alcohols, such as methanol and ethanol, the microscopic structure of the liquid phase is dominated in all regions by the hydrogen-bonded network of the headgroups.

C. Binary Mixture Phase Behavior. Alkanes and alcohols form highly nonideal mixtures that display vapor−liquid coexistence envelopes with maximum-pressure (minimum-boiling-point) azeotropes. In Figure 9, the pressure−composition diagrams for the binary system *n*-hexane/methanol at $T = 448.15$ K obtained from calculations for the TraPPE-UA and OPLS−UA force fields are compared to the experimental data.[66] The TraPPE-UA force field reproduces the shape of the experimental curve well but is shifted to higher pressures over the entire composition range. In comparison, the OPLS−UA force field yields a vapor pressure for neat *n*-hexane that is too low, whereas that for neat methanol is predicted to be too high.[67] The outcome is that the shape of the binary curve for the OPLS−UA force field deviates substantially from experiments. Of particular interest is the location of the azeotrope. The TraPPE-UA prediction of the azeotropic composition of $x_{hexane} = 0.340$ is in good agreement with the experimental value of $x_{hexane} = 0.288$, whereas the OPLS−UA force field yields a value of $x_{hexane} = 0.056$. The TraPPE-UA results for this mixture are comparable in accuracy to simulation results for the Errington-Panagiotopoulos exp-6 based methanol and *n*-hexane united-atom force fields.[59] The pressure−composition diagram for *n*-hexane/ethanol at $T = 413.15$ K is also presented in Figure 9. Again, the TraPPE-UA prediction of the azeotropic composi-

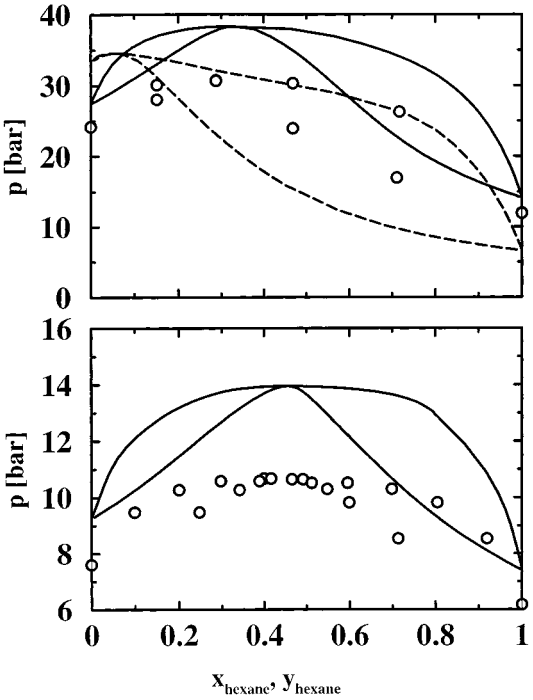

Figure 9. Pressure−composition diagrams for the binary mixtures of *n*-hexane/methanol at $T = 448.15$ K (top) and *n*-hexane/ethanol at $T = 413.15$ K (bottom). Experimental data[66,68] are depicted by circles, whereas the simulation results for the TraPPE-UA and OPLS-UA force fields are shown as solid and dashed lines, respectively.

tion of $x_{hexane} = 0.454$ is close to the experimental value of $x_{hexane} = 0.440$.[68]

The TraPPE-UA model yields azeotropic pressures of $P = 38.4$ and 13.95 bar for the *n*-hexane/methanol and *n*-hexane/ethanol mixtures, respectively. These values are about 30% higher than the experimental results of $P = 30.7$ and 10.66 bar, respectively. Because the pure component vapor pressures are over-predicted by as much as 20% by the TraPPE-UA alcohol and alkane force fields, the entire pressure composition diagram is expected to shift to higher pressures. Even accounting for this error, the azeotropic pressures are still too high, which is the result of the unlike-pair interaction between methanol or ethanol and hexane molecules being too weak. For the same reason, it can be observed that the composition gap between vapor and liquid phases is widened for the TraPPE-UA force field. Although the use of nonpolarizable models with fixed charges has been suggested as a possible cause for the disagreement between simulation and experiment[59] for the alkane/alcohol mixtures, it may be possible to improve the predictions of the mixture phase behavior through additional refinement of nonpolarizable models as has been recently demonstrated for alkane/carbon dioxide mixtures.[69]

In addition to the determination of phase boundaries, the histogram-reweighting methods allow for the calculation of the Gibbs free energies of transfer for each component between the mutually saturated vapor and the liquid phases over the entire pressure−composition diagram. In Figure 10, the Gibbs free energies of transfer from vapor phase to liquid phase are shown for the *n*-hexane/methanol mixture at 448.15 K. At the azeotrope, the Gibbs free energies of transfer for each component have to be equal, thus providing a useful method for locating the precise composition of the azeotrope. For comparison, we have also included the results of simulations of the OPLS−UA force field for *n*-hexane and methanol. Although a crossing point

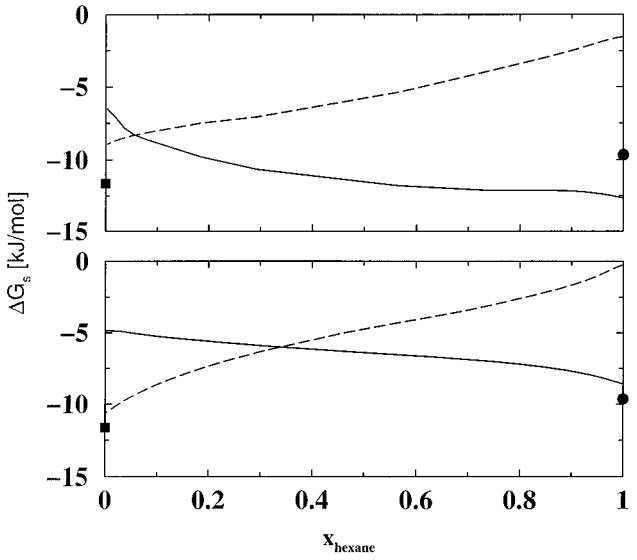

Figure 10. Gibbs free energies of transfer for *n*-hexane (solid lines) and methanol (dashed lines) from vapor to liquid phase for their mutually saturated mixtures at $T = 448.15$ K. Top (OPLS-UA), bottom (TraPPE-UA). Experimental results[60] for pure *n*-hexane and methanol are shown as filled circles and squares, respectively.

(azeotrope) is also present in this case, it occurs at a much lower x_{hexane} than for the TraPPE-UA force field or as found in experiment.

For the TraPPE-UA force field, the Gibbs free energies of transfer for a molecule between its own saturated liquid and vapor phases were determined to be −8.6 kJ/mol for *n*-hexane and −10.7 kJ/mol for methanol. These compare favorably with the experimental results of −9.7 and −11.6 kJ/mol for *n*-hexane and methanol, respectively.[60] Results for the OPLS−UA model for the pure component Gibbs free energies of transfer were calculated as −12.7 and −9.00 kJ/mol for *n*-hexane and methanol, respectively. These values suggest that the OPLS−UA force field is not correctly balanced in the sense that it predicts Gibbs free energies of transfer that are too large in magnitude for the *n*-alkanes, whereas the value for methanol is too small in magnitude.

Comparing the concentration dependencies of the Gibbs free energies of transfer of methanol and *n*-hexane calculated for the TraPPE-UA force field (see Figure 10), it is evident that the curve for *n*-hexane is fairly linear for $x_{hexane} < 0.8$, and the Gibbs free energy changes by only −4 kJ/mol from infinite dilution in methanol to pure *n*-hexane. In contrast, the corresponding curve for methanol shows a pronounced S-shape with larger concentration dependencies in the low and high concentration regimes (with a change of more than +10 kJ/mol from pure methanol to infinite dilution in *n*-hexane). Here, we would like to argue that the enhanced concentration effects close to $x_{hexane} = 0$ and 1 are caused by large structural rearrangements, that is, already the addition of a small amount of *n*-hexane results in a dramatic disruption of the hydrogen-bonded network of methanol molecules, and most methanol molecules are converted from aggregated states to a monomeric state at sufficient dilution ($0.8 < x_{hexane} \leq 0.9$).

D. Microscopic Structures of the Alkane/Alcohol Mixtures. Isothermal−isobaric simulations were used to investigate the structural properties of *n*-hexane/methanol mixtures at five points on the pressure composition diagram. Liquid-phase simulations were performed for pressures of 30.4, 35.8, 38.0, 38.4, and 35.4 bar. These conditions correspond to $x_{hexane} = 0.83$, 0.64, 0.46, 0.325, and 0.095, respectively. To learn about

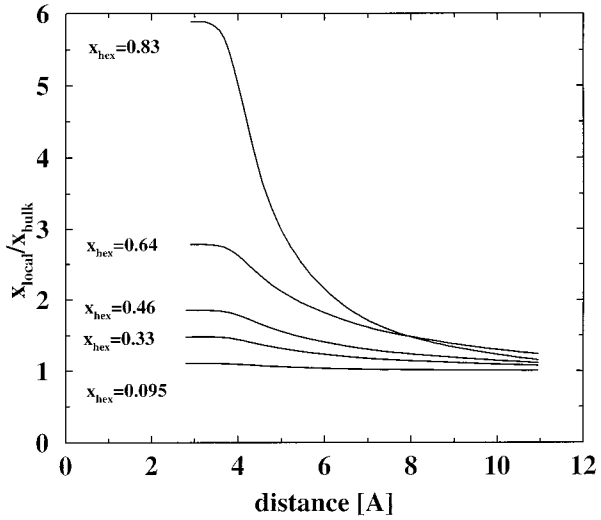

Figure 11. Liquid-phase local mole fraction enhancements in the vicinity of a methanol molecule calculated from center-of-mass radial distribution functions. The results, in order of decreasing hexane mole fraction, correspond to pressures of 30.4, 35.8, 38.0 (hexane-rich), 38.4 (azeotrope), and 35.4 bar (methanol-rich).

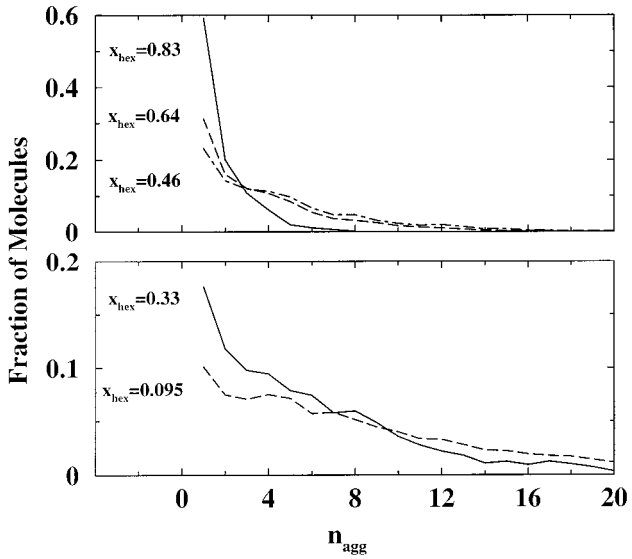

Figure 12. Fraction of molecules which belong to a cluster of a given aggregation number calculated for the liquid phases. The top part shows the cluster size distributions for $x_{hexane} > x_{hexane}^{azeotrope}$, whereas the bottom depicts the data for $x_{hexane} < x_{hexane}^{azeotrope}$. These mole fractions correspond to the same pressures as in Figure 11.

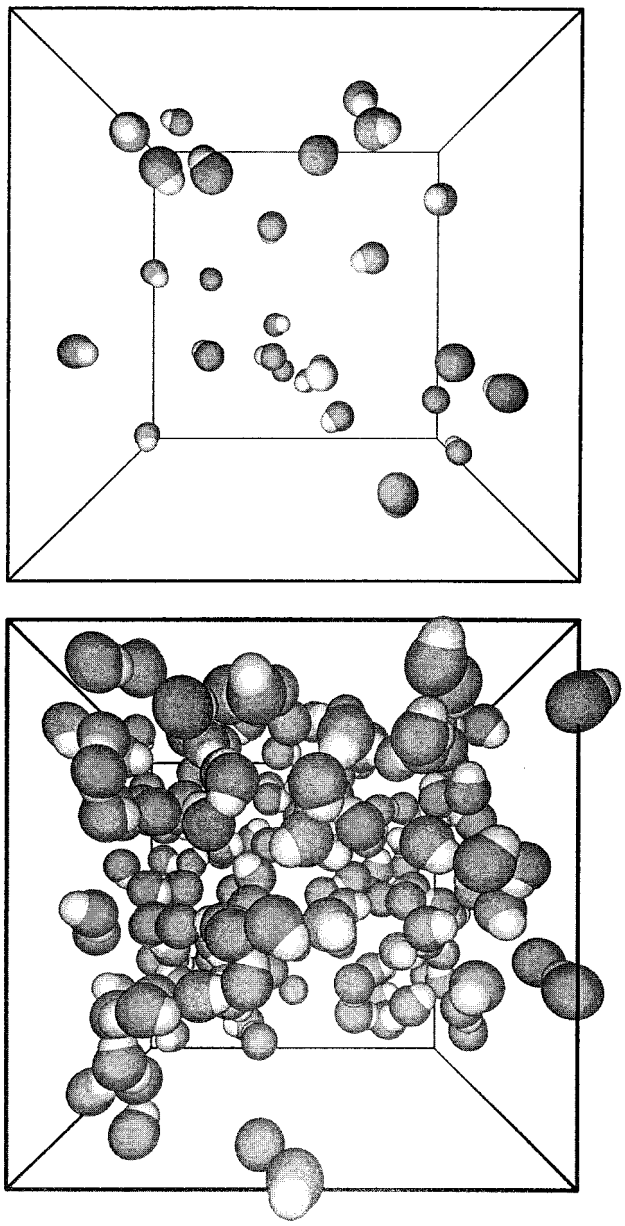

Figure 13. Snapshots of the liquid phases for the *n*-hexane/methanol system at $p = 30.4$ bar and $x_{hexane} = 0.83$ (top) and at $p = 35.4$ bar and $x_{hexane} = 0.095$ (bottom). The linear dimension of the periodic box is 37.78 Å for the former (top) and 28.34 Å for the latter (bottom). Dark and light spheres depict oxygen and hydrogen atoms, respectively. To improve clarity, all CH_2 and CH_3 groups have been omitted.

the microheterogeneity of this mixture, the local mole fractions were determined as functions of distance away from a tagged particle. The local mole fractions were calculated from the number integrals of the radial distribution functions, that is the average number of molecules of a given type up to a distance r away from the tagged molecule divided by the sum of the average numbers of molecules of any type. The local mole fraction enhancement is then defined as the local mole fraction divided by the bulk mole fraction. The enhancements of the local mole fraction of methanol molecules around a given methanol molecule versus distance are shown in Figure 11. For the hexane-rich phases, one finds a much higher concentration of methanol around other methanol molecules than in the bulk. As the bulk mole fraction of methanol increases, the local mole fraction enhancement approaches unity. This transition is continuous from hexane-rich to methanol-rich conditions. The presence of an azeotrope does not cause a discontinuity in the composition dependence of the local mole fraction enhancement. Although the local mole fraction enhancement is large for low concentrations of methanol in hexane, the number of nearest neighbor methanol molecules around a given methanol molecule is only about 0.5 for $x_{hexane} = 0.83$, whereas it approaches 2.0 for $x_{hexane} = 0.095$.

Examination of the cluster size distributions, Figure 12, shows that for the hexane-rich phase ($x_{hexane} = 0.83$), approximately 60% of the methanol molecules are not clustered. (Again, an O−O separation of 3.5 Å was used to determine aggregation.) Clusters consisting of two methanol molecules account for 20% of the total number of methanol molecules, while the remainder of methanol molecules are found in aggregates with three or more molecules. As the bulk concentration of methanol increases, the size of the clusters also increases. For methanol-

rich phases, more than half of the methanol molecules belong to larger aggregates with more than 8 molecules. The transition from a large number of small clusters to a small number of larger aggregates is smooth, with no discontinuity at the azeotropic composition.

In Figure 13, two snapshots of the system generated from a *NpT* simulations at pressures of 30.4 and 35.4 bar and with hexane mole fractions of 0.83 and 0.095, respectively, are shown. For low methanol concentrations, most of the methanol molecules are not aggregated or form dimers, as is also evident from the cluster distributions shown in Figure 12. As the concentration of methanol increases, chainlike aggregates begin to appear. At high concentrations of methanol, the majority of the methanol molecules can be found as part of chainlike aggregates, although some ring structures are also present. This differs significantly from simulations of dilute solutions of hexan-1-ol in *n*-hexane, where cyclic structures were found to be the predominant architectures of the aggregates and few, if any, linear chains were observed.[67] We speculate that the bulkiness of the long alkyl tails disfavors the formation of extended linear aggregates at low concentration.

5. Conclusions

The TraPPE-UA force field is extended to primary, secondary, and ternary alcohol by the introduction of new hydroxyl O and H, α-CH_3, α-CH_2, and α-CH pseudoatoms. The performance of the TraPPE-UA force field for the prediction of thermophysical properties is in general very satisfactory with mean unsigned errors of about 1% for the saturated liquid densities and normal boiling points and errors of 1.5 and 3% for the critical temperatures and densities, respectively. As also observed for alkanes,[25,26] alkenes and aromatics,[28] this force field tends to overpredict the saturated vapor pressures. The TraPPE-UA pseudo-atoms are transferable from one molecule type to another using the standard Lorentz−Berthelot combining rules for Lennard−Jones interactions of unlike pseudo-atoms. In addition, it is found that the TraPPE-UA force field predicts the azeotropic compositions for the binary alkane/alkanol mixtures rather well but the azeotropic pressures are overestimated and the phase envelopes are slightly wider than their experimental counterparts. This deviation is in part caused by the united-atom approximation of the alkyl tail (which yields vapor pressures that are too high for the pure systems) and by the limitation of nonpolarizable models, which results in an underestimation of the interactions between unlike molecules.

Structural analysis of the liquid phases showed that for all neat alcohols on average two hydrogen bonds are formed per hydroxyl group. An increase in the alkyl chain length and/or bulkiness leads to smaller cluster sizes in the liquid phase. Whereas the hydrogen-bonded network of hydroxyl groups is locally ordered, the tail segments of the longer alcohols form an isotropic environment. Significant aggregation of methanol molecules was observed for the *n*-hexane/methanol mixtures. Enhancements of the local mole fraction of methanol molecules around other methanol molecules are most pronounced at low methanol concentrations. The liquid structure at the azeotropic point does not show any special features.

Acknowledgment. We thank Stan Sandler for stimulating discussions. Financial support from the National Science Foundations (CTS-9813601), a Sloan Research Fellowship, a Doctoral Dissertation Fellowship (B.C.), and a Minnesota Supercomputing Institute Research Scholarship (J.J.P.) is gratefully acknowledged. Part of the computer resources were provided by the Minnesota Supercomputing Institue.

References and Notes

(1) Marcus, Y. *The Properties of Solvents*; John Wiley Sons: Chichester, 1998.
(2) Schuster, P.; Zundel, G.; Sandorfy, C. *The Hydrogen Bond*; North-Holland: Amsterdam, 1976; Vol. 1−3.
(3) Zachariasen, W. H. *J. Chem. Phys.* **1935**, *3*, 158.
(4) Harvey, G. G. *J. Chem. Phys.* **1938**, *6*, 111.
(5) Wertz, D. L.; Kruh, R. K. *J. Chem. Phys.* **1967**, *47*, 388.
(6) Mikusinska-Planner, A. *Acta Crystallogr., Sect. A: Cryst. Phys. Diffr., Theor. Gen. Crystallogr.* **1977**, *A33*, 433.
(7) Narten, A. H.; Sandler, S. I. *J. Chem. Phys.* **1979**, *71*, 2069.
(8) Montague, D. G.; Gibson, I. P.; Dore, J. C. *Mol. Phys.* **1981**, *44*, 1355; Montague, D. G.; Gibson, I. P.; Dore, J. C. *Mol. Phys.* **1982**, *47*, 1405.
(9) Magini, M.; Paschina, G,; Piccaluga, G. *J. Chem. Phys.* **1982**, *77*, 2051.
(10) Symons, M. C. R. *Chem. Soc. Rev.* **1983**, *12*, 1.
(11) Narten, A. H.; Habenschuss, A. *J. Chem. Phys.* **1984**, *80*, 3387.
(12) Vcij, J. K.; Reid, C. J.; Evans, M. W. *Mol. Phys.* **1983**, *50*, 935.
(13) Jorgensen, W. L. *J. Phys. Chem.* **1986**, *90*, 1276.
(14) Haughney, M.; Ferrario, M.; McDonald, I. R. *J. Phys. Chem.* **1987**, *91*, 4934.
(15) Matsumoto, M.; Gubbins, K. E. *J. Chem. Phys.* **1990**, *93*, 1981.
(16) van Leeuwen, M. E.; Smit, B. *J. Phys. Chem.* **1995**, *99*, 1831.
(17) van Leeuwen, M. E. *Mol. Phys.* **1996**, *87*, 87.
(18) González, M. A.; Enciso, E.; Bermejo, F. J.; Bée, M. *J. Chem. Phys.* **1999**, *110*, 8045.
(19) Errington, J. R.; Panagiotopoulos, A. Z.; Potoff, J. J. in *AIChE 1999 Annual Meeting*, paper 73i.
(20) Marcus, Y. J. *Solution Chem.* **1990**, *19*, 507−517.
(21) Hansch, C.; Fujita, T. *J. Am. Chem. Soc.* **1964**, *86*, 1616.
(22) Kamlet, M. J.; Abraham, M. H.; Doherty, R. M.; Taft, R. W. *J. Am. Chem. Soc.* **1984**, *106*, 464.
(23) Sangster, J. *Octanol−Water Partition Coefficients: Fundamentals and Physical Chemistry*; John Wiley Sons: Chichester, 1997.
(24) Siepmann, J. I.; Karaborni, S.; Smit, B. *Nature* **1993**, *365*, 330.
(25) Martin, M. G.; Siepmann, J. I. *J. Phys. Chem. B* **1998**, *102*, 2569.
(26) Martin, M. G.; Siepmann, J. I. *J. Phys. Chem. B* **1999**, *103*, 4508.
(27) Chen, B.; Siepmann, J. I. *J. Phys. Chem. B* **1999**, *103*, 5370.
(28) Wick, C. D.; Martin, M. G.; Siepmann, J. I. *J. Phys. Chem. B* **2000**, *104*, 8008.
(29) Longuet-Higgins, H. C.; Salem, L. *Proc. Royal Soc. London* **1961**, *A259*, 433.
(30) Amos, A. T.; Crispin, R. J. In T*heoretical Chemistry: Advances and Perspectives*; Eyring, H., Henderson, D., Eds.; Academic: New York, 1976, Vol. 2, pp 2;.
(31) Kaplan, I. G. *Theory of Molecular Interactions, Translation*; Fraga, S.; Klobukowski, M., Eds.; Elsevier Science Publishers: Tarrytown, New York, 1986.
(32) Badenhoop, J. K.; Weinhold, F. *J. Chem. Phys.* **1997**, *107*, 5422.
(33) Lorentz, H. A. *Annalen Phys.* **1881**, *12*, 127.
(34) Berthelot, D. *C. (r) Hebd. Séanc. Acad. Sci., Paris* **1898**, *126*, 1703.
(35) Van der Ploeg, P.; Berendsen, A. *J. Chem. Phys.* **1982**, *76*, 3271.
(36) Cornell, W. D.; Cieplak, P.; Bayly, C.; Gould, I. R.; Merz, K. M.; Ferguson, D. M.; Spellmeyer, D. C.; Fox, T.; Caldwell, J. W.; Kollman, P. A. *J. Am. Chem. Soc.* **1995**, *117*, 5179.
(37) Jorgensen, W. L.; Madura, J. D.; Swenson, C. J. *J. Am. Chem. Soc.* **1984**, *106*, 813.
(38) Lide, D. A. *CRC Handbook of Chemistry and Physics*; CRC Press: Boca Raton, 1991.
(39) Gregory, J. K.; Clary, D. C.; Liu, K.; Brown, M. G.; Saykally, R. J. *Science* **1997**, *275*, 814.
(40) Chen, B.; Xing, J.; Siepmann, J. I. *J. Phys. Chem. B* **2000**, *104*, 2391; and references therein.
(41) Panagiotopoulos, A. Z. *Mol. Phys.* **1987**, *61*, 813.
(42) Panagiotopoulos, A. Z.; Quirke, N.; Stapleton, M.; Tildesley, D. J. *Mol. Phys.* **1988**, *63*, 527.
(43) Smit, B.; de Smedt, P.; Frenkel, D. *Mol. Phys.* **1989**, *68*, 931.
(44) Siepmann, J. I. *Mol. Phys.* **1990**, *70*, 1145.
(45) Siepmann, J. I.; Frenkel, D. *Mol. Phys.* **1992**, *75*, 59.
(46) Frenkel, D.; Mooij, G. C. A. M.; Smit, B. *J. Phys.: Cond. Matt.* **1992**, *4*, 3053.
(47) de Pablo, J. J.; Laso, M.; Suter, U. W. *J. Chem. Phys.* **1992**, *96*, 2395.
(48) Vlugt, T. J. H.; Martin, M. G.; Smit, B.; Siepmann, J. I.; Krishna, R. *Mol. Phys.* **1998**, *94*, 727.
(49) Wood, W. W.; Parker, F. R. *J. Chem. Phys.* **1955**, *27*, 720.
(50) Allen, M. P.; Tildesley, D. J. *Computer Simulation of Liquids*; Oxford University Press: Oxford, 1987.

(51) Chen, B.; Siepmann, J. I. *J. Phys. Chem. B* **1999**, *103*, 5370.
(52) Esselink, K.; Loyens, L. D. J. C.; Smit, B. *Phys. Rev. E* **1995**, *51*, 1560.
(53) Mackie, A. D.; Tavitian, B.; Boutin, A.; Fuchs, A. H. *Mol. Simul.* **1997**, *19*, 1.
(54) Ferrenberg, A. M.; Swendsen, R. H. *Phys. Rev. Lett.* **1988**, *61*, 2635.
(55) Ferrenberg, A. M.; Swendsen, R. H. *Phys. Rev. Lett.* **1989**, *63*, 1195.
(56) Swendsen, R. H. *Physica A* **1993**, *194*, 53.
(57) Errington, J. R.; Panagiotopoulos, A. Z. *J. Chem. Phys.* **1998**, *109*, 1093.
(58) Potoff, J. J.; Panagiotopoulos, A. Z. *J. Chem. Phys.* **1998**, *109*, 10 914.
(59) Potoff, J. J.; Errington, J. R.; Panagiotopoulos, A. Z. *Mol. Phys.* **1999**, *97*, 1073.
(60) Smith, B. D.; Srivastava, R. *Thermodynamic Data for Pure Compounds: Part B Halogenated Hydrocarbons and Alcohols*; Elsevier: Amsterdam, 1986.
(61) Experimental coexistence densities for pentane-1,5-diol could not be found but liquid densities at standard pressure are available for a few temperatures below the boiling point.[60] Therefore, we performed some additional simulations in the isothermal−isobaric ensemble to determine the specific liquid densities for pentane-1,5-diol (also shown in Figure 1).
(62) Smit, B.; Williams, C. P. *J. Phys.: Condens. Matter* **1990**, *2*, 4281.
(63) Rowlinson, J. S.; Swinton, F. L. *Liquids and Liquid Mixtures*, 3rd ed.; Butterworth: London, 1982.
(64) Pitzer, K. S. *J. Phys. Chem.* **1995**, *99*, 13 070.
(65) Wilding, N. B. *Phys. Rev. E* **1995**, *52*, 602.
(66) Zawisza, A. J. *Chem. Thermodynamics* **1985**, *17*, 941.
(67) Stubbs, J. M.; Chen, B.; Potoff, J. J.; Siepmann, J. I. *Fluid Phase Equil.* **2001**, in press.
(68) Nhu, N. V.; Liu, A.; Sauermann, P.; Kohler, F. *Fluid Phase Equil.* **1998**, *145*, 269.
(69) Potoff, J. J.; Siepmann, J. I. *AIChE J.* **2001**, in press.